

Detecting train driveshaft damages using accelerometer signals and Differential Convolutional Neural Networks

Antía López Galdo^{a,*}, Alejandro Guerrero-López^{a,b,*}, Pablo M. Olmos^{a,b}, María Jesús Gómez García^c

^a*Department of Signal Processing and Communications, Universidad Carlos III de Madrid, Leganés, 28911, Spain*

^b*Instituto de Investigación Sanitaria Gregorio Marañón, Madrid, 28007, Spain*

^c*Department of Mechanical Engineering, Universidad Carlos III de Madrid, Leganes, 28911, Spain*

Abstract

Railway axle maintenance is critical to avoid catastrophic failures. Nowadays, condition monitoring techniques are becoming more prominent in the industry to prevent enormous costs and damage to human lives.

This paper proposes the development of a railway axle condition monitoring system based on advanced 2D-Convolutional Neural Network (CNN) architectures applied to time-frequency representations of vibration signals. For this purpose, several preprocessing steps and different types of Deep Learning (DL) and Machine Learning (ML) architectures are discussed to design an accurate classification system. The resultant system converts the railway axle vibration signals into time-frequency domain representations, i.e., spectrograms, and, thus, trains a two-dimensional CNN to classify them depending on their cracks. The results showed that the proposed approach outperforms several alternative methods tested. The CNN architecture has been tested in 3 different wheelset assemblies, achieving AUC scores of 0.93, 0.86, and 0.75 outperforming any other architecture and showing a high level of reliability when classifying 4 different levels of defects.

Keywords: Condition monitoring; Vibration signal; Crack detection; Railway axles; Deep Learning; Convolutional Neural Networks

2010 MSC: 00-01, 99-00

1. Introduction

In industry, the development of new technologies and the trend towards process automation have opened up new lines of research, such as maintenance prediction [1, 2] or estimation of remaining bearing life [3, 4]. In terms of

*Equally contributed

Email address: alexjorguer@tsc.uc3m.es (Alejandro Guerrero-López)

maintenance, condition-based maintenance is essential in industrial processes to achieve high system safety, reliability, and availability [5, 6].

Condition monitoring aims to continuously monitor and report on the condition of a machine during operation. Knowing the standard operating patterns is crucial to detect disturbances and take the appropriate action; therefore, recent studies are focused on this field [7, 8, 9, 10]. This type of maintenance implies that the machine is stopped only when necessary, thus reducing costs and time and increasing productivity.

The dynamic behaviour of rotating machines in the presence of a defect has been studied in detail in recent decades. More specifically, with respect to railway axles, the literature [11, 12, 13, 14, 15] points out that vibration signals provide important information about their mechanical performance. Since the breakage of such an element can lead to a very critical situation, the interest in this field has grown. Many types of cracks can appear in an axle, depending on their shape, direction, and evolution.

In the field of condition monitoring applied to railway equipment, several studies have been focused on monitoring the condition of track and bearings [16, 17]. Other studies analyzed the wheel wear phenomena [18, 19], and the wheel crack detection [20]. Traditionally, non-destructive testing techniques were used, based on the complete disassembly of the units to carry out functional tests. However, recent publications are beginning to study the modelling of cracked railway axles with a fault-tolerant approach and crack propagation models [21, 22]. Others, study their dynamic behavior [23, 24], whereas other authors propose to automatically detect cracks [25, 26, 27, 28].

Deep Learning (DL) is a branch of Machine Learning (ML) based on the implementation of Artificial Neural Networks (ANN) for the extraction and transformation of characteristics based on significant volumes of data. Deep Neural Network (NN)s are considered hierarchical and multilayered architectures used to extract valuable knowledge from vast amounts of data and use it for classification or regression goals. The crucial features that distinguish NNs from any other algorithm are the non-linearity between input and output data and the application of the backpropagation algorithm [29] to optimize the objective function. These ANNs are classified according to the purpose and characteristics of the system. In short, DL is a technique that enables algorithms to learn from experience and data, taking advantage of ANN and multilayer nonlinear processing units. DL has contributed to analyzing automatically fault diagnosis and crack classification. In [30], an attention recurrent autoencoder with Long-Short Term Memory (LSTM)s was proposed to extract time-dependent features from one-dimensional vibration signals. A similar approach was developed in [31], where an attention-based-LSTM and a Random Forest (RF) were used to predict time series trends based on relevant characteristics extracted by wavelet packet analysis. Other authors used auto-encoder models [32] applied to time-frequency spectrograms to locate worn crossings in railway servicing. In other studies, such as [33], proposed to use Generative Adversarial Networks (GAN) combined with **LSTM!** (**LSTM!**)s to predict the temperature of a high-speed train axle in long-term forecasting. A different approach for automatic failure recognition

in photovoltaic systems by thermographic images was proposed in [34] through the usage of Convolutional Neural Network (CNN)s. The application of CNNs for identifying failures using vibration sensors was further developed in [35] where the aim of alerting when maintenance tasks need to be carried out. From both [30, 35] we followed the idea of no preprocessing the data with wavelet analysis [31]. However, we propose not following their approach to dealing with time dependencies, such as LSTMs [30, 31], or 1D-CNN [31] models. Thus, we propose to use images, that is, a time-frequency representation of the vibration signals.

Therefore, this paper proposes the introduction of a railway axle condition monitoring system based on advanced 2D-CNN architectures applied to time-frequency representations of vibration signals. We introduce a differential CNN structure that captures the statistical properties of the system and enables generalization. This is a critical novelty in the state-of-the-art and a step forward in condition monitoring systems, improving safety, and reducing costs by extending current inspection intervals. To demonstrate this, several experiments were performed on three Wheelset Assemblies (WA) with different test conditions. In each WA, four types of cracks were tested (no crack, 5.7mm, 10.9mm, 15mm), and classification AUCs of 0.93, 0.86, and 0.75, over each WA respectively, were reported. Thus, improving state-of-the-art methods, such as LSTM [30, 31], 1D-CNNs [35], and RF [31].

The code for reproducing all the experiments proposed in this paper is provided ¹.

The article is organised as follows: Section 2 details the experimental system, the conditions under which the tests were performed, and the main characteristics of the vibration signals obtained. Section 3 describes the data preprocessing phase, the model structure, and the selected hyperparameters. In Section 4 the results of our approach and graphical interpretation are provided. Finally, in Section 5 some final remarks are given.

2. Experimental design

The railway axle’s vibration signals were acquired experimentally, investigating the dynamics of cracked rotors with an experimental system in which full-scaled railway axles were placed [26, 27]. A bogie test rig was used to build this experimental system. The test rig comprises a fixed bench and a drive system for rolling the axles. It also incorporates a loading system that uses hydraulic actuators to apply a vertical load to the bogie. During the test, the load selected remains constant, replicating real-world situations. The real experimental setup is shown in Fig. 1.

The tests were carried out for 3 WAs, called WA1, WA2, and WA3, thus creating 3 different datasets. For all WAs, the test conditions shown in Table 1 were tested.

¹<https://github.com/antialopezg/Crack-detection-railway-axles-deep-learning>



Figure 1: Bogie framework.

Test condition	Values			
Flaw condition	Healthy shaft (D0)	5.7mm (D1)	10.9mm (D2)	15mm (D3)
Load	4t	10t		
Speed	20 km/h	50 km/h		
Wheelsets rotation	Counterclockwise	Clockwise		
Axle box accelerometer orientation	Axial	Lengthwise	Vertical	
Axle box accelerometer place	RHS	LHS		

Table 1: Conditions tested for each WA.

First, the axle was tested without cracks for each of the assemblies tested. Subsequently, without disassembling the axle, three different crack sizes (5.7mm, 10.9mm, and 15mm, called D1, D2, and D3, respectively) were induced in the central section of the axle. The applied load and speed remained invariant during the tests, replicating natural stationary conditions displayed in Table 1. Each axle box had three uniaxial accelerometer sensors oriented in three directions; two radial directions, vertical and horizontal in the direction of motion, and the axial direction in the direction of the axis. Thus, a total of six accelerometers are set. Furthermore, the rotation of the wheelset was tested in both senses of rotation.

Vibration signals were acquired using a sampling frequency of 12.8 kHz and 16384 points, resulting in signals of duration of 1.28 s. Then, 58063 temporal vibration signal samples were obtained and distributed as shown in Table 2.

Dataset	# Observations	# D0	# D1 (5.7mm)	# D2 (10.9mm)	# D3 (15mm)
WA1	12955	4762	2323	2940	2930
WA2	20757	5220	5203	5551	4783
WA3	11395	2996	3001	3292	2106

Table 2: Datasets description. The total number of samples per dataset and their decomposition by each level of defect.

3. Differential convolutional model

3.1. Data preprocessing

The vibration signals were reduced to one turn of rotation, subsampled to 2000 points, and normalised. These signals were used in our experiments in two ways: as a raw temporal 1D signal and also converted into the time-frequency domain, via a spectrogram, to explore the 2D spatial correlation. Since the data were transferred to the time-frequency domain, for each vibration signal, a 3-channel image was obtained representing the spectrogram’s real, imaginary and magnitude information, as shown in Fig. 2 for an example.

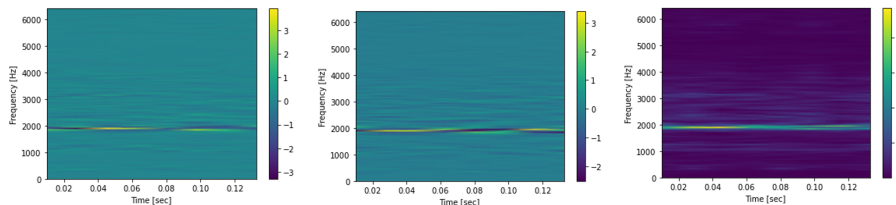


Figure 2: Spectrogram representation of a vibration signal a) real part, b) imaginary part, c) magnitude.

Then, each of the 4 different defects was categorised, creating a categorical target: no Defect (D0), Defect 1 5.7mm (D1), Defect 2 10.9mm (D2), and Defect 3 15mm (D3). Data related to the axial direction were discarded as it was found to be not informative in previous studies.

According to the standards, to perform vibration analysis, it is necessary to measure in all three directions (axial, vertical, and longitudinal). However, from what was seen in practice both in this case and in previous studies, such as [27], the effects of cracking in this direction are much less visible than in the other directions. This has also been observed from numerical simulations [23]. Therefore, only the radial directions of the axle are normally used for this type of system, [22, 36, 27]. To reduce the computational cost, the axial direction data were excluded.

Once the data was preprocessed and cleaned, it was divided into three partitions: training, validation, and testing. As shown in Table 3, for training, only data corresponding to WA1 was used, specifically 50% of the available data. A 30% of WA1’s data was used for validation. Finally, both the remaining 20%

Training	Validation	Testing		
WA1	WA1	WA1	WA2	WA3
7255	3109	2591	20757	11395

Table 3: Data used for each step in the models. The first row indicates from which WA is the data while the second row indicates the number of samples used for each purpose.

of WA1 data and all data acquired from WA2 and WA3 were tested to evaluate whether the model can generalise to a WA never seen.

3.2. Model architecture

The proposed model combined 6 layers of 2D-CNN with a Multilayer Perceptron (MLP) as a classifier as shown in Fig. 3. Namely, we used a two-dimensional CNN network with 6 convolutional layers of 6, 16, 26, 36, 46, 56 channel size with a kernel size of 2, a stride of 1, and padding *same*. After the convolutional layers, there was a dropout layer to prevent the network from overfitting. We have not performed exhaustive hyperparameter validation. As such, all of our results can be potentially refined.

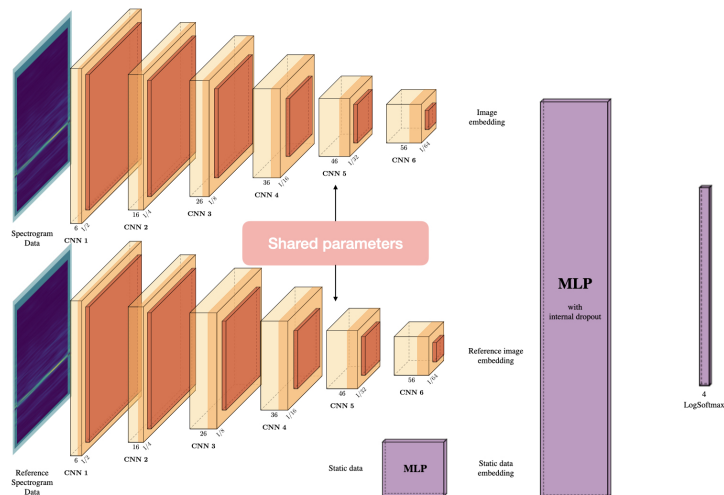


Figure 3: Model architecture. Each convolutional layer follows a 2×2 MaxPooling layer, hence, the image is divided by two at each layer. There are three inputs: the spectrograms, the reference spectrograms, and the static data. Thus, three embeddings are calculated. Finally, they are all fused to compute the four possible defects: D0, D1, D2, and D3.

To improve generalisation, we have designed a differential approach in which the classifier has two inputs. On the one hand, the spectrogram of the signal to classify. On the other hand, the spectrogram of a reference *healthy* signal axle, is measured at the beginning of the experiment before any axle damage is

performed. In this way, we enforce the network to learn the differences between defective and healthy railway axles. Note that the same CNN is used in both branches, i.e., the parameters are shared. That is, feature extraction is common for both signals. Therefore, a fraction of the dataset is left as a reference, i.e., it was essential to randomly extract data corresponding to the healthy shaft so that the system can know the experiments' initial conditions and distinguish between the defects.

As shown in Fig. 3, the static characteristics of the signals were processed through an MLP with 5 input features (since we had 5 static variables, see Table 1), and 10 output features, one for each possible value of the variables. Finally, the vibrations feature vector and the static characteristics feature vector were fused by a fully connected layer with a log-softmax activation function that classified each vibration signal between D0, D1, D2, or D3. Also, a dropout layer is added to prevent overfitting.

Through cross-validation, the optimal values for both learning rate and dropout were chosen to be 0.001 and 0.7, respectively.

This article tested different architectures based on different interpretations of the data provided as baselines to compare our proposal. Following the state-of-the-art, we designed and tested other architectures. First, following the literature [30, 31] sequential NNs were implemented, such as LSTM [37]. LSTMs are a variant of Recurrent Neural Network (RNN) that relies on a gated cell to track information through many steps. Therefore, LSTMs can control the information flow [38]. As other authors proposed [35], a 1D-CNNs intended for sequential processing [39] was also proposed. Furthermore, we also tested the combination of both using a 1D-CNN plus and LSTM where the 1D-CNN is applied to the vibration signal to exploit the time dependency and a unit cell LSTM was included after the CNN layers to control the information flow over time following the structure shown in Fig. 4.

Moreover, following the literature [31], we also used preprocessing packages intended to signal processing such as *tsfresh* [40] followed by ML classifiers. To make a fair comparison with our differential learning, we tested with and without healthy references in all the previous models. Furthermore, we compared our differential learning approach with domain adaptation methods such as *KMM* [41] and *TAB* [41] followed by ML classifiers. These domain adaptation methods are intended to help generalise the models by adapting the new signal seen to the healthy signals of that domain, performing a similar idea to our differential learning approach. In Table 6 we have compared all these approaches to ours in average performance. To see the detailed results of each baseline, see Appendix A.

4. Results

Each railway axle vibration signal depends on the conditions tested (place, load, rotation, orientation and speed), which takes two possible values each. Therefore, there are $2^5 = 32$ possible combinations of these characteristics for which the performance of the models was tested. This performance is evaluated

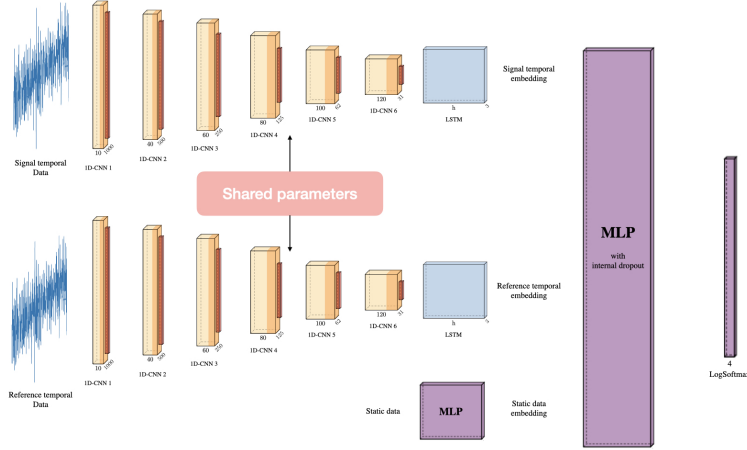


Figure 4: 1D-CNN LSTM baseline architecture. There are three inputs: the signals, the reference signals, and the static data. Thus, three embeddings are calculated. Finally, they are all fused to compute the four possible defects: D0, D1, D2, and D3.

using the Area Under the Curve Receiver Operating Characteristics (AUROC). The AUROC shows the evolution of the false positive ratio versus the true positive ratio or recall, where a 1 indicates a perfect classification of all signals.

Table 4 shows the AUROC performance for every possible combination of test conditions. As shown, WA1 presented the highest performance, reaching the perfect classification in two configurations. However, WA3 was the most difficult to classify, although no configuration is below 0.66 AUROC performance.

Table 5 shows the summary of Table 4 for each condition. When increasing speed, see *Speed 50 km/h* row, it is easier to detect the cracks in the WA1 but it does not improve in the other two WA. Let us remark on the *Counterclockwise* configuration, where it is perfectly generalisable for WA2, achieving similar results as in WA1 but it is the worst performance for WA3. In summary, it is shown that generalising to WA3 is harder in any configuration.

Table 6 also shows the performance of all baselines compared to the proposed model. As baselines, different approaches were taken. First, the *tsfresh* preprocessing package was used to extract autocorrelated features. Then, it was combined with different classifiers such as Logistic Regressor (LR), RF, or Support Vector Machines (SVM). Then, domain adaptation was proposed to help the generalization. For this purpose, Kernel Mean Matching (KMM) was proposed as an unsupervised domain adaptation method, and TrAdaBoost (TAB) was used as a supervised method. In TAB, healthy railway signals were used as a reference. Further details can be found at Appendix A. As shown, TAB-LR-Ref performs slightly better in WA3. However, both 1D-CNN-LSTM-Ref and 2D-CNN-Ref outperform all methods, achieving the best overall mean

Place	Orientation	Rotation	Load	Speed	AUROC WA1	AUROC WA2	AUROC WA3
0 = RHS 1 = LHS	0 = Lengthwise 1 = Vertical	0 = Counterclockwise 1 = Clockwise	0 = 5t 1 = 10t	0 = 20 km/h 1 = 50 km/h			
0	0	0	0	0	0.845	0.896	0.797
0	0	0	0	1	0.954	0.943	0.699
0	0	0	1	0	0.75	0.917	0.692
0	0	0	1	1	0.962	0.919	0.727
1	0	0	0	0	0.891	0.869	0.821
1	0	0	0	1	0.907	0.895	0.7
1	0	0	1	0	0.909	0.858	0.698
1	0	0	1	1	0.933	0.894	0.795
0	0	1	0	0	0.895	0.87	0.768
0	0	1	0	1	0.998	0.838	0.772
0	0	1	1	0	0.93	0.9	0.762
0	0	1	1	1	0.997	0.823	0.832
1	0	1	0	0	0.94	0.832	0.775
1	0	1	0	1	0.969	0.886	0.782
1	0	1	1	0	0.952	0.805	0.779
1	0	1	1	1	1	0.793	0.669
0	1	0	0	0	0.885	0.923	0.741
0	1	0	0	1	0.985	0.917	0.682
0	1	0	1	0	0.752	0.927	0.688
0	1	0	1	1	0.914	0.855	0.785
1	1	0	0	0	0.96	0.906	0.806
1	1	0	0	1	0.973	0.823	0.629
1	1	0	1	0	0.915	0.901	0.702
1	1	0	1	1	0.972	0.794	0.764
0	1	1	0	0	0.904	0.872	0.754
0	1	1	0	1	0.992	0.814	0.778
0	1	1	1	0	0.916	0.809	0.789
0	1	1	1	1	0.994	0.841	0.704
1	1	1	0	0	0.919	0.795	0.743
1	1	1	0	1	0.995	0.77	0.902
1	1	1	1	0	0.926	0.851	0.752
1	1	1	1	1	1	0.849	0.806

Table 4: Results for the classification of the 4 possible defects present in each WA. Each row represents a different test condition scenario. The AUROC columns represent the mean AUROC value scored for the classification of the 4 different defects present in each WA.

performance.

Fig. 5 and Fig. 6 show the ROC curves for training and validation over WA1, respectively. Then, Figs. 7, 8, and 9 show testing ROC curves for each WA, classifying the 4 different defects. The proposed model differs between healthy (D0) and defective axles (D1, D2, D3), in all datasets achieving 0.89, 0.85, and 0.79 AUROC scores in each WA, respectively. Furthermore, the system also detects the deepest defect (D3) with an AUROC score of 0.80, 0.85, and 0.77 in each WA, respectively.

5. Conclusion

The results concluded that the 1D-CNN-LSTM and 2D-CNN networks are suitable for the diagnosis of cracks in railway axle vibration signals. However, due to the high complexity of dealing with time signals, the 2D-CNN was finally chosen. This solution involves translating the time signals into the time-frequency domain to evaluate spectrograms with image classification methods.

The results showed that the 2D-CNN architecture outperformed several alternative methods tested. In the first place, preprocessing techniques such as the *tsfresh* [40] package or domain adaptation packages [41] such as KMM or TAB

Test condition	Value	AUROC WA1	AUROC WA2	AUROC WA3
Place	RHS	0.91 \pm 0.08	0.88 \pm 0.05	0.75 \pm 0.05
	LHS	0.95 \pm 0.03	0.85 \pm 0.04	0.76 \pm 0.06
Orientation	Lengthwise	0.93 \pm 0.07	0.87 \pm 0.04	0.76 \pm 0.05
	Vertical	0.88 \pm 0.16	0.82 \pm 0.06	0.76 \pm 0.07
Rotation	Counterclockwise	0.91 \pm 0.07	0.89 \pm 0.04	0.73 \pm 0.05
	Clockwise	0.96 \pm 0.04	0.83 \pm 0.04	0.77 \pm 0.05
Load	5t	0.94 \pm 0.05	0.87 \pm 0.05	0.76 \pm 0.06
	10t	0.93 \pm 0.08	0.86 \pm 0.05	0.75 \pm 0.05
Speed	20 km/h	0.89 \pm 0.06	0.87 \pm 0.04	0.75 \pm 0.04
	50 km/h	0.97 \pm 0.03	0.85 \pm 0.05	0.76 \pm 0.07

Table 5: Summary of Table 4 for each condition. Each value represents the mean and standard deviation w.r.t. AUROC for each value of each condition.

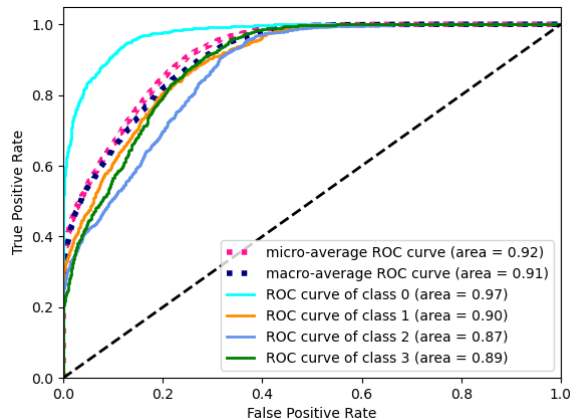


Figure 5: Training ROC curve over WA1.

was proven not to be needed. Therefore, 2D-CNN outperformed all baselines and eliminated time-consuming preprocessing steps. Therefore, exploiting the spatial correlation of the spectrograms of the railway axle vibration signals allows the diagnosis of railway axle cracks. Second, it was proved necessary to include the reference information on the WA in which the vibration signals were generated to generalise to any setup. In this way, information was passed on about the state of the healthy axle, allowing the system to distinguish healthy behaviour from defective one.

In future work, we will analyze which regions of the spectrogram influence the classifier’s decision by including attention models, also known as Transformers [42].

Model	WA1	WA2	WA3	Overall
<i>tsfresh</i> -LR	0.77	0.55	0.65	0.66
<i>tsfresh</i> -SVM	0.77	0.57	0.66	0.67
<i>tsfresh</i> -RF	0.88	0.45	0.48	0.69
KMM-LR	0.77	0.64	0.64	0.68
KMM-SVM	0.77	0.57	0.62	0.65
KMM-RF	0.79	0.61	0.65	0.68
2D-CNN (no reference)	0.93	0.56	0.46	0.65
TAB-LR-Ref	0.76	0.71	0.80	0.76
TAB-SVM-Ref	0.77	0.69	0.71	0.72
TAB-RF-Ref	0.76	0.66	0.69	0.70
1D-CNN-LSTM-Ref	0.89	0.86	0.79	0.85
2D-CNN-Ref	0.93	0.86	0.75	0.85

Table 6: Mean AUROC performance for all possible test conditions in each WA of the proposed model and all baselines presented in Appendix A. The **Ref** label indicates whether the healthy signal of reference was used.

Acknowledgments

This work has been developed within the project Sistema de monitorización de estado para detección de fisuras en ejes ferroviarios (SMEPDFEF-CM-UC3M), 2021 Call for grants to carry out interdisciplinary R&D projects for young doctors of the Carlos III University from Madrid. The work was also supported by MCIN AEI [grant numbers RTI2018-099655-B-100 and PID2021-123182OB-I00]; by the Comunidad de Madrid [grant numbers IND2022/TIC-23550]; by the European Union (FEDER and the European Research Council (ERC) through the European Unions Horizon 2020 research innovation program [grant number 714161]; and by the IISGM [grant INTRAMURAL].

References

- [1] D. Mourtzis, E. Vlachou, A cloud-based cyber-physical system for adaptive shop-floor scheduling and condition-based maintenance, *Journal of Manufacturing Systems* 47 (2018) 179–198. doi:10.1016/j.jmsy.2018.05.008.
- [2] K. T. Nguyen, K. Medjaher, A new dynamic predictive maintenance framework using deep learning for failure prognostics, *Reliability Engineering and System Safety* 188 (2019) 251–262. doi:10.1016/j.ress.2019.03.018.
- [3] X. Li, W. Zhang, Q. Ding, Deep learning-based remaining useful life estimation of bearings using multi-scale feature extraction, *Reliability Engineering and System Safety* 182 (2019) 208–218. doi:10.1016/j.ress.2018.11.011.

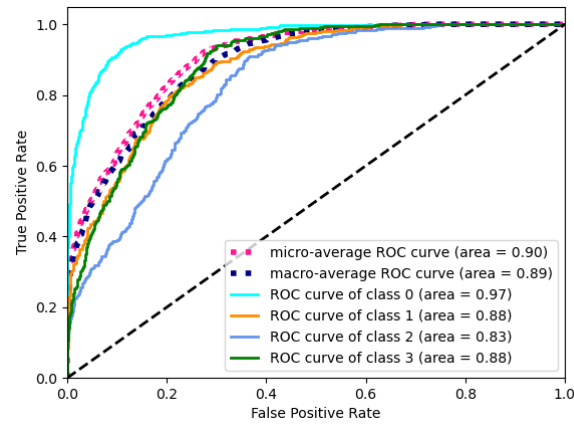


Figure 6: Validation ROC curve over WA1.

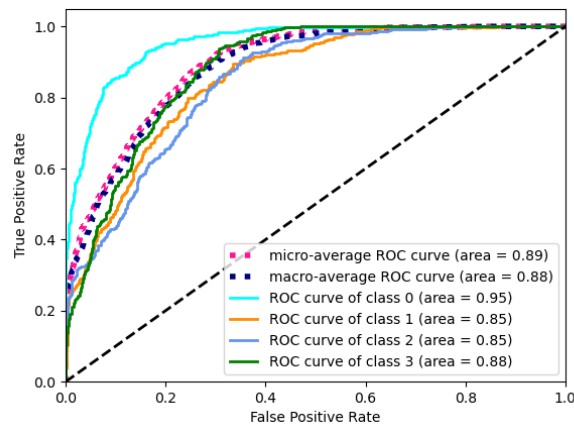


Figure 7: Testing ROC curve over WA1.

- [4] Y. Ding, M. Jia, Q. Miao, P. Huang, Remaining useful life estimation using deep metric transfer learning for kernel regression, *Reliability Engineering ; System Safety* 212 (2021) 107583. doi:10.1016/j.res.2021.107583.
- [5] The use of sensor based technology for enhancing maintenance operations, *Advances in Manufacturing Technologies and Production Engineering* (2022) 89–100doi:10.2174/9789815039771122010012.
- [6] Y. Lu, L. Sun, X. Zhang, F. Feng, J. Kang, G. Fu, Condition based maintenance optimization for offshore wind turbine considering opportunities based on neural network approach, *Applied Ocean Research* 74 (2018) 69–79. doi:10.1016/j.apor.2018.02.016.

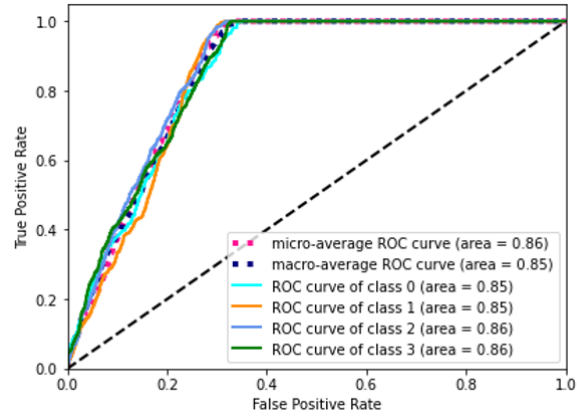


Figure 8: Testing ROC curve over WA2.

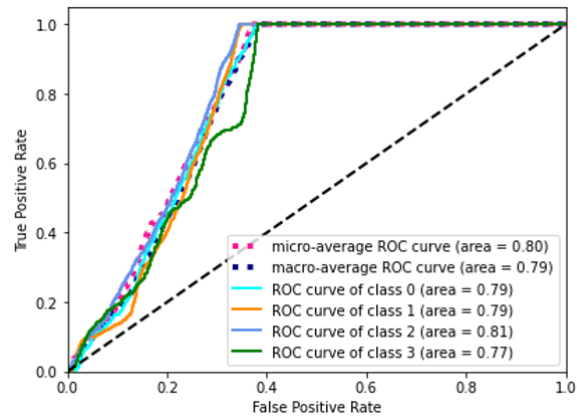


Figure 9: Testing ROC curve over WA3.

- [7] W. YAO, X. LI, Pitch system fault diagnosis for wind turbine based on condition monitoring, *Renewable energy resources* 34 (3) (2016) 437–440.
- [8] Y. Pan, R. Hong, J. Chen, Z. Qin, Y. Feng, Incipient fault detection of wind turbine large-size slewing bearing based on circular domain, *Measurement* 137 (2019) 130–142.
- [9] Z. Liu, L. Zhang, J. Carrasco, Vibration analysis for large-scale wind turbine blade bearing fault detection with an empirical wavelet thresholding method, *Renewable Energy* 146 (2020) 99–110.
- [10] L. Zhang, F. Zhang, Z. Qin, Q. Han, T. Wang, F. Chu, Piezoelectric energy harvester for rolling bearings with capability of self-powered condition monitoring, *Energy* 238 (2022) 121770.

- [11] T. W. Rauber, A. L. da Silva Loca, F. d. Boldt, A. L. Rodrigues, F. M. Varejão, An experimental methodology to evaluate machine learning methods for fault diagnosis based on vibration signals, *Expert Systems with Applications* 167 (2021) 114022. doi:10.1016/j.eswa.2020.114022.
- [12] H. Sohn, C. R. Farrar, Damage diagnosis using time series analysis of vibration signals, *Smart Materials and Structures* 10 (3) (2001) 446–451. doi:10.1088/0964-1726/10/3/304.
- [13] X. Zhang, Z. Zhao, Z. Wang, X. Wang, Fault detection and identification method for quadcopter based on airframe vibration signals, *Sensors* 21 (2) (2021) 581. doi:10.3390/s21020581.
- [14] S. Han, N. Mannan, D. C. Stein, K. R. Pattipati, G. M. Bollas, Classification and regression models of audio and vibration signals for machine state monitoring in precision machining systems, *Journal of Manufacturing Systems* 61 (2021) 45–53. doi:10.1016/j.jmsy.2021.08.004.
- [15] Z. Ye, J. Yu, Deep morphological convolutional network for feature learning of vibration signals and its applications to gearbox fault diagnosis, *Mechanical Systems and Signal Processing* 161 (2021) 107984. doi:10.1016/j.ymsp.2021.107984.
- [16] J. A. Silmon, C. Roberts, Improving railway switch system reliability with innovative condition monitoring algorithms, *Proceedings of the Institution of Mechanical Engineers, Part F: Journal of Rail and Rapid Transit* 224 (4) (2010) 293–302. doi:10.1243/09544097jrtr313.
- [17] M. Entezami, C. Roberts, P. Weston, E. Stewart, A. Amini, M. Papaalias, Perspectives on railway axle bearing condition monitoring, *Proceedings of the Institution of Mechanical Engineers, Part F: Journal of Rail and Rapid Transit* 234 (1) (2019) 17–31. doi:10.1177/0954409719831822.
- [18] F. Braghin, S. Bruni, F. Resta, Wear of railway wheel profiles: A comparison between experimental results and a mathematical model, *Vehicle System Dynamics* 37 (2003) 478–489. doi:10.1080/00423114.2002.11666256.
- [19] F. Braghin, R. Lewis, R. Dwyer-Joyce, S. Bruni, A mathematical model to predict railway wheel profile evolution due to wear, *Wear* 261 (2006) 1253–1264. doi:10.1016/j.wear.2006.03.025.
- [20] A. Alemi, F. Corman, G. Lodewijks, Condition monitoring approaches for the detection of railway wheel defects, *Proceedings of the Institution of Mechanical Engineers, Part F: Journal of Rail and Rapid Transit* 231. doi:10.1177/0954409716656218.
- [21] A. Pourheidar, S. Beretta, D. Ragazzi, C. Baykara, Comparison of sif solutions for cracks under rotating bending and their impact upon propagation lifetime of railway axles, *Procedia Structural Integrity* 8 (2018) 610–617. doi:10.1016/j.prostr.2017.12.060.

- [22] S. Beretta, F. Sangalli, J. Syeda, D. Panggabean, J. Rudlin, Raai project: Life-prediction and prognostics for railway axles under corrosion-fatigue damage, *Procedia Structural Integrity* 4 (2017) 64–70. doi:10.1016/j.prostr.2017.07.010.
- [23] M. Hassan, S. Bruni, M. Carboni, Crack detection in railway axle using horizontal and vertical vibration measurements (2016) 1–6doi:10.1049/cp.2016.1190.
- [24] P. Rolek, S. Bruni, M. Carboni, Condition monitoring of railway axles based on low frequency vibrations, *International Journal of Fatigue* 86 (2016) 88–97. doi:10.1016/j.ijfatigue.2015.07.004.
- [25] M. Gómez, C. Castejón, J. García-Prada, New stopping criteria for crack detection during fatigue tests of railway axles, *Engineering Failure Analysis* 56 (2015) 530–537. doi:10.1016/j.engfailanal.2014.10.018.
- [26] M. Gómez, E. Corral, C. Castejón, J. García-Prada, Effective crack detection in railway axles using vibration signals and wpt energy, *Sensors* 18 (5) (2018) 1603. doi:10.3390/s18051603.
- [27] M. J. Gómez, C. Castejón, E. Corral, J. C. García-Prada, Railway axle condition monitoring technique based on wavelet packet transform features and support vector machines, *Sensors* 20 (12) (2020) 3575. doi:10.3390/s20123575.
- [28] R.-V. Sánchez, P. Lucero, J.-C. Macancela, H. Rubio Alonso, M. Cerrada, D. Cabrera, C. Castejón, Evaluation of time and frequency condition indicators from vibration signals for crack detection in railway axles, *Applied Sciences* 10 (12) (2020) 4367. doi:10.3390/app10124367.
- [29] S. Wang, J. Di, D. Wang, X. Dai, Y. Hua, X. Gao, A. Zheng, J. Gao, State-of-the-art review of artificial neural networks to predict, characterize and optimize pharmaceutical formulation, *Pharmaceutics* 14 (1). doi:10.3390/pharmaceutics14010183.
URL <https://www.mdpi.com/1999-4923/14/1/183>
- [30] X. Kong, X. Li, Q. Zhou, Z. Hu, C. Shi, Attention recurrent autoencoder hybrid model for early fault diagnosis of rotating machinery, *IEEE Transactions on Instrumentation and Measurement* 70 (2021) 1–10. doi:10.1109/TIM.2021.3051948.
- [31] H. Xu, R. Ma, L. Yan, Z. Ma, Two-stage prediction of machinery fault trend based on deep learning for time series analysis, *Digital Signal Processing* 117 (2021) 103150. doi:10.1016/j.dsp.2021.103150.
- [32] J. Silva-Rodríguez, P. Salvador, V. Naranjo, R. Insa, Supervised contrastive learning-guided prototypes on axle-box accelerations for railway crossing inspections, *Expert Systems with Applications* 207 (2022) 117946.

- [33] J. Man, H. Dong, J. Gao, J. Zhang, L. Jia, Y. Qin, Ga-grgat: A novel deep learning model for high-speed train axle temperature long term forecasting, *Expert Systems with Applications* 202 (2022) 117033.
- [34] D. Manno, G. Cipriani, G. Ciulla, V. Di Dio, S. Guarino, V. Lo Brano, Deep learning strategies for automatic fault diagnosis in photovoltaic systems by thermographic images, *Energy Conversion and Management* 241 (2021) 114315. doi:10.1016/j.enconman.2021.114315.
- [35] R. M. Souza, E. G. Nascimento, U. A. Miranda, W. J. Silva, H. A. Lepikson, Deep learning for diagnosis and classification of faults in industrial rotating machinery, *Computers & Industrial Engineering* 153 (2021) 107060. doi:10.1016/j.cie.2020.107060.
- [36] M. Gómez, C. Castejón, J. García-Prada, Automatic condition monitoring system for crack detection in rotating machinery, *Reliability Engineering and System Safety* 152 (2016) 239–247. doi:10.1016/j.res.2016.03.013.
- [37] S. Hochreiter, J. Schmidhuber, Long short-term memory, *Neural computation* 9 (8) (1997) 1735–1780.
- [38] S. Kalla, *Neural networks* (05 2021).
URL <https://medium.com/nerd-for-tech/neural-networks-68531432fb5>
- [39] R. Khandelwal, *Convolutional neural network: Feature map and filter visualization* (05 2020).
URL <https://towardsdatascience.com/convolutional-neural-network-feature-map-and-filter-visualization-f75012a5a49c>
- [40] M. Christ, N. Braun, J. Neuffer, A. W. Kempa-Liehr, Time series feature extraction on basis of scalable hypothesis tests (tsfresh – a python package), *Neurocomput.* 307 (C) (2018) 72–77. doi:10.1016/j.neucom.2018.03.067.
URL <https://doi.org/10.1016/j.neucom.2018.03.067>
- [41] A. de Mathelin, F. Deheeger, G. Richard, M. Mougeot, N. Vayatis, *Adapt: Awesome domain adaptation python toolbox*, arXiv preprint arXiv:2107.03049.
- [42] A. Vaswani, N. Shazeer, N. Parmar, J. Uszkoreit, L. Jones, A. N. Gomez, Ł. Kaiser, I. Polosukhin, Attention is all you need, *Advances in neural information processing systems* 30.

Appendix A. Additional experiments

Other architectures were designed to test the effectiveness and reliability of the results obtained with the 2D-CNNs:

- **Not reference-based evaluation:** the input into 2D-CNN was only the spectrogram to be classified without the reference of a healthy axle.
- **1DCNN + LSTM:** the vibration signal was used in the time domain, that is, no spectrogram was used. A 1D-CNN is applied to the vibration signal to exploit the time dependency. A LSTM unit cell was included after the CNN layers to control the information flow over time.
- ***Tsfresh* [40] feature extraction and ML classifier:** the *tsfresh* library was used to extract features from temporal signals and reduce dimensionality. These features were used as input to different classifiers such as an LR, an SVM, or an RF.
- ***KMM* [41] unsupervised domain adaptation and ML classifier:** the unsupervised KMM method was used to adapt the domain using reference healthy signals unlabeled. This new domain was used as input to different classifiers such as an LR, an SVM, or an RF.
- ***TAB* [41] supervised domain adaptation and ML classifier:** the supervised KMM method was used to adapt the domain using reference healthy signals labelled. This new domain was used as input to different classifiers such as an LR, an SVM, or an RF.

Appendix A.1. Results

Results by configuration and dataset are displayed in terms of AUROC for each of the three approaches.

Appendix A.1.1. Not references

As shown in Table A.1.1, the mean AUROC for WA1 was 0.93, as in the proposal of the main document. However, the mean AUROC was 0.56 and 0.46 for WA2 and WA3, respectively, which implies that if we omitted the reference spectrograms in the NN, it was not able to generalise to different WA. In other words, the system needs information about the healthy axle to distinguish the initial configuration and thus identify defects.

Appendix A.1.2. 1D-CNN-LSTM

Table A.1.2 shows a similar performance to the main proposal presented in the article. The mean AUROC was 0.89, 0.86, and 0.79 for WA1, WA2 and WA3, respectively. However, the overall mean AUROC for the 1D-CNN-LSTM case was 0.855, while the 2D-CNN was 0.867. Therefore, 2D-CNN is more generalised.

In addition, images are easy to handle with a CNN that exploits spatial correlation.

Place	Orientation	Rotation	Load	Speed	AUROC WA1	AUROC WA2	AUROC WA3
0 = RHS 1 = LHS	0 = Lengthwise 1 = Vertical	0 = Counterclockwise 1 = Clockwise	0 = 5t 1 = 10t	0 = 20 km/h 1 = 50 km/h			
0.0	0.0	0.0	0.0	0.0	0.867	0.682	0.676
0.0	0.0	0.0	0.0	1.0	0.978	0.673	0.42
0.0	0.0	0.0	1.0	0.0	0.836	0.781	0.326
0.0	0.0	0.0	1.0	1.0	0.977	0.776	0.194
1.0	0.0	0.0	0.0	0.0	0.902	0.625	0.498
1.0	0.0	0.0	0.0	1.0	0.992	0.447	0.468
1.0	0.0	0.0	1.0	0.0	0.819	0.7	0.29
1.0	0.0	0.0	1.0	1.0	0.987	0.549	0.679
0.0	0.0	1.0	0.0	0.0	0.928	0.65	0.47
0.0	0.0	1.0	0.0	1.0	1.0	0.438	0.417
0.0	0.0	1.0	1.0	0.0	0.925	0.652	0.489
0.0	0.0	1.0	1.0	1.0	0.998	0.445	0.664
1.0	0.0	1.0	0.0	0.0	0.907	0.442	0.528
1.0	0.0	1.0	0.0	1.0	0.996	0.349	0.757
1.0	0.0	1.0	1.0	0.0	0.87	0.439	0.487
1.0	0.0	1.0	1.0	1.0	0.999	0.598	0.597
0.0	1.0	0.0	0.0	0.0	0.864	0.64	0.354
0.0	1.0	0.0	0.0	1.0	0.999	0.392	0.493
0.0	1.0	0.0	1.0	0.0	0.831	0.639	0.226
0.0	1.0	0.0	1.0	1.0	0.957	0.457	0.398
1.0	1.0	0.0	0.0	0.0	0.895	0.648	0.583
1.0	1.0	0.0	0.0	1.0	1.0	0.502	0.498
1.0	1.0	0.0	1.0	0.0	0.835	0.667	0.219
1.0	1.0	0.0	1.0	1.0	0.995	0.55	0.446
0.0	1.0	1.0	0.0	0.0	0.877	0.465	0.378
0.0	1.0	1.0	0.0	1.0	1.0	0.381	0.186
0.0	1.0	1.0	1.0	0.0	0.89	0.591	0.491
0.0	1.0	1.0	1.0	1.0	0.99	0.643	0.563
1.0	1.0	1.0	0.0	0.0	0.931	0.657	0.51
1.0	1.0	1.0	0.0	1.0	0.998	0.285	0.729
1.0	1.0	1.0	1.0	0.0	0.86	0.62	0.491
1.0	1.0	1.0	1.0	1.0	0.999	0.521	0.334

Table A.1.1: AUROC results non referenced-based model.

Appendix A.1.3. Feature extraction and a Machine Learning classifier

The last experiment consisted of two phases. The first phase, the feature extraction step, was based on the use of the *tsfresh* library to extract and select relevant features from the signals and use them as input to the classifier instead of the vibration signal. The second phase consisted of performing cross-validation to train a Random Forest classifier and evaluate this model in each possible configuration.

As seen in Table A.1.3, this model does not generalise to the rest of the datasets, so there was a lot of overfitting. The mean AUROC per dataset was much lower than in previous cases, being 0.88, 0.45, and 0.48 for WA1, WA2 and WA3, respectively.

Place	Orientation	Rotation	Load	Speed	AUROC WA1	AUROC WA2	AUROC WA3
0 = RHS 1 = LHS	0 = Lengthwise 1 = Vertical	0 = Counterclockwise 1 = Clockwise	0 = 5t 1 = 10t	0 = 20 km/h 1 = 50 km/h			
0.0	0.0	0.0	0.0	0.0	0.818	0.907	0.769
0.0	0.0	0.0	0.0	1.0	0.887	0.884	0.715
0.0	0.0	0.0	1.0	0.0	0.765	0.889	0.84
0.0	0.0	0.0	1.0	1.0	0.893	0.913	0.718
1.0	0.0	0.0	0.0	0.0	0.86	0.87	0.882
1.0	0.0	0.0	0.0	1.0	0.889	0.864	0.634
1.0	0.0	0.0	1.0	0.0	0.907	0.89	0.863
1.0	0.0	0.0	1.0	1.0	0.869	0.9	0.841
0.0	0.0	1.0	0.0	0.0	0.882	0.902	0.765
0.0	0.0	1.0	0.0	1.0	0.954	0.834	0.817
0.0	0.0	1.0	1.0	0.0	0.925	0.85	0.81
0.0	0.0	1.0	1.0	1.0	0.937	0.844	0.814
1.0	0.0	1.0	0.0	0.0	0.922	0.858	0.828
1.0	0.0	1.0	0.0	1.0	0.942	0.841	0.833
1.0	0.0	1.0	1.0	0.0	0.908	0.805	0.785
1.0	0.0	1.0	1.0	1.0	0.897	0.796	0.762
0.0	1.0	0.0	0.0	0.0	0.859	0.898	0.797
0.0	1.0	0.0	0.0	1.0	0.876	0.895	0.728
0.0	1.0	0.0	1.0	0.0	0.799	0.887	0.869
0.0	1.0	0.0	1.0	1.0	0.804	0.882	0.801
1.0	1.0	0.0	0.0	0.0	0.971	0.917	0.824
1.0	1.0	0.0	0.0	1.0	0.888	0.932	0.702
1.0	1.0	0.0	1.0	0.0	0.933	0.883	0.868
1.0	1.0	0.0	1.0	1.0	0.873	0.925	0.668
0.0	1.0	1.0	0.0	0.0	0.896	0.827	0.75
0.0	1.0	1.0	0.0	1.0	0.925	0.866	0.79
0.0	1.0	1.0	1.0	0.0	0.885	0.816	0.818
0.0	1.0	1.0	1.0	1.0	0.986	0.825	0.75
1.0	1.0	1.0	0.0	0.0	0.916	0.881	0.781
1.0	1.0	1.0	0.0	1.0	0.916	0.881	0.855
1.0	1.0	1.0	1.0	0.0	0.873	0.786	0.836
1.0	1.0	1.0	1.0	1.0	0.904	0.81	0.809

Table A.1.2: AUROC results 1D-CNN-LSTM model.

Place	Orientation	Rotation	Load	Speed	AUROC WA1	AUROC WA2	AUROC WA3
0 = RHS 1 = LHS	0 = Lengthwise 1 = Vertical	0 = Counterclockwise 1 = Clockwise	0 = 5t 1 = 10t	0 = 20 km/h 1 = 50 km/h			
0.0	0.0	0.0	0.0	0.0	0.892	0.365	0.506
0.0	0.0	0.0	0.0	1.0	0.899	0.407	0.535
0.0	0.0	0.0	1.0	0.0	0.875	0.46	0.505
0.0	0.0	0.0	1.0	1.0	0.874	0.451	0.526
1.0	0.0	0.0	0.0	0.0	0.855	0.436	0.493
1.0	0.0	0.0	0.0	1.0	0.885	0.498	0.513
1.0	0.0	0.0	1.0	0.0	0.87	0.437	0.474
1.0	0.0	0.0	1.0	1.0	0.898	0.491	0.481
0.0	0.0	1.0	0.0	0.0	0.835	0.452	0.416
0.0	0.0	1.0	0.0	1.0	0.913	0.414	0.478
0.0	0.0	1.0	1.0	0.0	0.936	0.451	0.467
0.0	0.0	1.0	1.0	1.0	0.872	0.441	0.451
1.0	0.0	1.0	0.0	0.0	0.875	0.461	0.496
1.0	0.0	1.0	0.0	1.0	0.858	0.489	0.486
1.0	0.0	1.0	1.0	0.0	0.858	0.423	0.465
1.0	0.0	1.0	1.0	1.0	0.88	0.456	0.486
0.0	1.0	0.0	0.0	0.0	0.86	0.41	0.515
0.0	1.0	0.0	0.0	1.0	0.884	0.442	0.434
0.0	1.0	0.0	1.0	0.0	0.856	0.441	0.486
0.0	1.0	0.0	1.0	1.0	0.903	0.473	0.494
1.0	1.0	0.0	0.0	0.0	0.915	0.454	0.438
1.0	1.0	0.0	0.0	1.0	0.908	0.471	0.444
1.0	1.0	0.0	1.0	0.0	0.89	0.476	0.494
1.0	1.0	0.0	1.0	1.0	0.929	0.448	0.476
0.0	1.0	1.0	0.0	0.0	0.906	0.48	0.545
0.0	1.0	1.0	0.0	1.0	0.923	0.464	0.49
0.0	1.0	1.0	1.0	0.0	0.895	0.451	0.498
0.0	1.0	1.0	1.0	1.0	0.837	0.433	0.5
1.0	1.0	1.0	0.0	0.0	0.873	0.478	0.526
1.0	1.0	1.0	0.0	1.0	0.872	0.492	0.457
1.0	1.0	1.0	1.0	0.0	0.853	0.457	0.449
1.0	1.0	1.0	1.0	1.0	0.827	0.465	0.526

Table A.1.3: AUROC results Random Forest model.